Coupled carbon and nitrogen cycling regulates the cnidarian-algal symbiosis

Nils Rädecker[1*], Stéphane Escrig[1], Jorge E. Spangenberg[2], Christian R. Voolstra[3], Anders Meibom[1,4]

[1] Laboratory for Biological Geochemistry, School of Architecture, Civil and Environmental Engineering, École Polytechnique Fédérale de Lausanne (EPFL), Lausanne, Switzerland

[2] Institute of Earth Surface Dynamics, University of Lausanne, Lausanne, Switzerland

[3] Department of Biology, University of Konstanz, Konstanz, Germany

[4] Center for Advanced Surface Analysis, Institute of Earth Sciences, University of Lausanne, Lausanne, Switzerland

* to whom correspondence should be addressed: nils.radecker@epfl.ch

ORCID iDs

Nils Rädecker	Stéphane Escrig	Jorge E. Spangenberg	Christian R. Voolstra	Anders Meibom
0000-0002-2387-8567	NA	0000-0001-8636-6414	0000-0003-4555-3795	0000-0002-4542-2819

Keywords

Aiptasia | endosymbiosis regulation | nutrient cycling | photosymbiosis | resource competition | Symbiodiniaceae

Author contributions

N.R conceived and conducted the experiment. N.R., S.E., and J.S. performed sample and data analysis. All authors contributed to writing and revising the manuscript.

Conflict of interest

The authors declare no competing interests.

Funding

N.R. and A.M. are supported by the Swiss National Science Foundation, grants 200021_179092 and 205321_212614.

Data availability

All associated data are available at zenodo.org.

Abstract

Efficient nutrient recycling underpins the ecological success of the cnidarian-algal symbiosis in oligotrophic waters that forms the basis of coral reef ecosystems. In a stable symbiosis, nitrogen limitation restricts the growth of algal endosymbionts and stimulates their release of photosynthates to the cnidarian animal host. However, the detailed mechanisms controlling nitrogen availability *in hospite* and their role in symbiosis regulation remain poorly understood. Here, we studied the metabolic regulation of symbiotic nitrogen cycling in the sea anemone Aiptasia by experimentally altering labile carbon availability in a series of experiments. Using isotope labeling experiments and NanoSIMS imaging, we show that the competition for environmental ammonium between the host and its algal symbionts is regulated by carbon availability. Light regimes that were optimal for algal photosynthesis increased carbon availability in the holobiont and enhanced symbiotic competition for nitrogen. Consequently, algal symbiont densities were lowest under optimal environmental conditions and increased toward the tolerance limits of the symbiosis. This metabolic regulation promotes efficient carbon recycling in a stable symbiosis across a wide range of environmental conditions. At the same time, the dependence on resource competition can favor parasitic interactions that may explain the instability of the symbiosis as the environmental conditions in the Anthropocene shift towards its tolerance limits.

Introduction

Photosymbioses between heterotrophic hosts and phototrophic symbionts are diverse and widespread in the aquatic environment (1). The efficient recycling of organic and inorganic nutrients in these associations provides a key advantage under oligotrophic conditions and has enabled their repeated evolutionary formation (2, 3). Coral reefs, with their immense biodiversity and productivity, are testimony to this ecological success and the fundamental role of photosymbioses in the marine environment (4, 5). Yet, the dependence of these ecosystems on the cnidarian-algal symbiosis may also prove their Achilles heel in times of global change. Marine heatwaves, among other environmental disturbances, now repeatedly cause the disruption of this symbiosis in so-called mass bleaching events that result in widespread ecosystem degradation (6). Thus, understanding the processes that maintain the stable cnidarian-algal symbiosis could shine a light on the evolutionary origins of photosymbioses and help understand their apparent susceptibility to the accelerating environmental change of the Anthropocene.

The regulation of the cnidarian-algal symbiosis is directly linked to the nutrient exchange between the host and its symbionts (7). In this symbiosis, the release of excess photosynthates by the algae supports the metabolic energy demands of the host (8). Host respiration in turn enhances CO_2 availability for algal photosynthesis, thereby forming an efficient recycling loop that supports high gross productivity (9). Constant nutrient limitation is required to initiate and maintain carbon translocation and recycling in the symbiosis (10, 11). In a stable state, low nitrogen availability limits algal symbiont growth and ensures the translocation of excess carbon to the host (12–14). Consequently, the onset of nitrogen limitation has been proposed to play a key role in the establishment of the cnidarian-algal symbiosis as it promotes life stage transition and controls the population density of the algal endosymbionts (15–17). Likewise, failure to maintain nitrogen-limited conditions has been linked to the breakdown of the symbiosis during heat stress, i.e., bleaching (18, 19).

However, while the importance of nitrogen cycling in the regulation of the cnidarian-algal symbiosis is widely accepted, the factors regulating nitrogen availability *in hospite* remain poorly understood (20, 21). Previous studies proposed that algal symbiont nitrogen limitation arises from symbiont-symbiont as well as host-symbiont competition for inorganic nitrogen (15, 22–25). However, the nutritional and environmental controls of these interactions and their role in regulating the symbiosis are largely unknown. Using the photosymbiotic model organism Aiptasia (26, 27), we conducted two

complementary experiments to elucidate the role of nitrogen competition in shaping symbiotic interactions. First, we investigated the role of labile carbon availability for host ammonium assimilation and its consequence on nitrogen availability for algal symbionts. Secondly, we tested how different light intensities affect symbiotic nitrogen competition and the resulting eco-evolutionary dynamics in photosymbioses.

Results & Discussion

Labile carbon availability limits ammonium assimilation in the cnidarian host metabolism

In the cnidarian-algal symbiosis, the host and its algal symbionts have the cellular machinery to use carbon backbones from the tricarboxylic acid (TCA) cycle for amino acid synthesis by fixing ammonium via the glutamate metabolism (Fig. 1A) (28, 29). Carbon translocation by algal symbionts could thus enhance nitrogen assimilation by their host (10, 23, 30). However, the metabolic controls of host ammonium fixation and its consequences for algal symbiont nitrogen uptake remain largely speculative (14, 20, 21, 31). Here, we investigated the effects of pyruvate addition on ammonium assimilation in aposymbiotic (algal symbiont-free) and photosymbiotic (algal symbiont-bearing) Aiptasia. As pyruvate is predominantly assimilated by the host and algal symbionts have limited access to and/or lack the cellular machinery to utilize this carbon source (32, 33), this approach allowed us to alter the relative carbon availability for symbiotic partners. Briefly, animals were isotopically labeled with $^{15}NH_4^+$ during 6 h incubations with or without 10 mM pyruvate addition and ^{15}N uptake was assessed using NanoSIMS imaging. Consistent with previous reports (34), aposymbiotic Aiptasia showed significantly less ammonium assimilation than their photosymbiotic counterparts (ANOVA, $F=131.6$, $p < 0.001$; Fig. 1B-I). However, pyruvate addition caused a pronounced increase in aposymbiotic ammonium assimilation (Tukey HSD, $p < 0.001$ for epidermis and gastrodermis, respectively) to levels resembling those of photosymbiotic Aiptasia. Likewise, pyruvate addition also enhanced ammonium assimilation in photosymbiotic Aiptasia, yet this effect was restricted to the gastrodermal tissue, i.e., the tissue hosting the algal symbionts (Tukey HSD, $p = 0.769$ for the epidermis and $p < 0.001$ for the gastrodermis).

Importantly, algal symbiont ammonium assimilation showed the reversed pattern with significantly reduced ^{15}N-enrichment following pyruvate addition (Tukey HSD, $p < 0.001$). These contrasting effects of pyruvate addition on the host and algal symbiont ammonium assimilation likely reflect their contrasting carbon utilization. Our results show that the uptake (and recycling) of ammonium by the host is limited by labile carbon availability; here pyruvate. While this limitation appears to be most pronounced in aposymbiotic animals, even photosymbiotic hosts were able to utilize the additional carbon source for their amino acid synthesis. Consequently, under our experimental conditions (i.e., after one week of starvation) algal symbiont photosynthate translocation appears to be insufficient to fully satisfy the metabolic carbon requirements of their host in a stable symbiosis with Aiptasia. The observed reduction in ammonium assimilation by algal symbionts during pyruvate addition is thus likely a direct consequence of increased host anabolic activity. These results suggest that symbiotic partners compete for ammonium and that the outcome of this competition is directly linked to carbon availability.

Taken together, these findings imply that a positive feedback loop regulates nutrient cycling in the symbiosis: translocation of algal photosynthates stimulates anabolic ammonium assimilation by their host. Reduced nitrogen availability for algal symbionts limits their growth and further enhances photosynthate translocation to the host. Environmental conditions affecting algal photosynthetic performance and/or organic nutrient pollution could thus directly alter nitrogen availability for algal symbionts because of changes in carbon availability in the host metabolism.

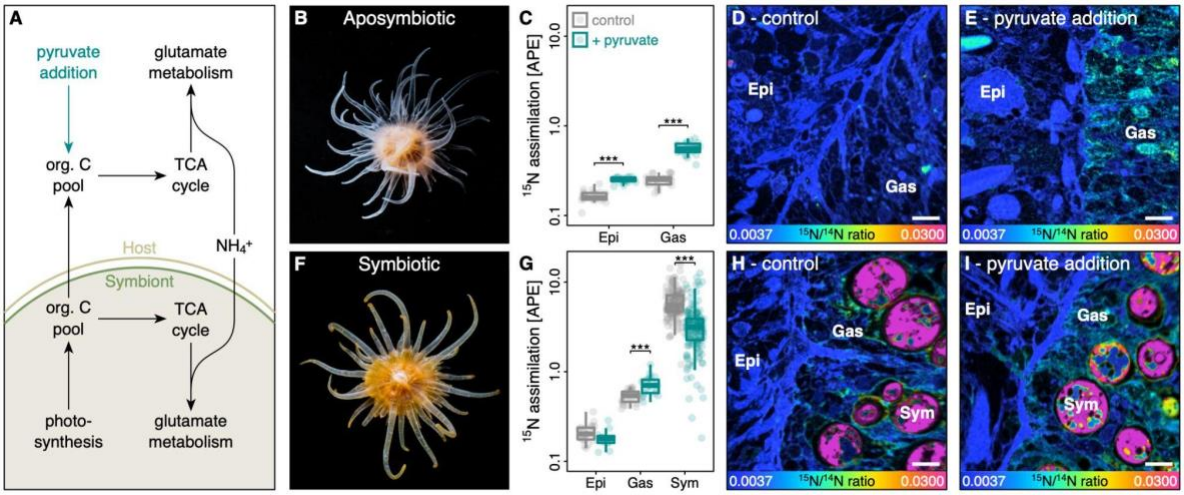

Fig. 1 | Effects of labile carbon availability on ammonium (NH_4^+) assimilation in Aiptasia. (A) Amino acid synthesis by the host and its algal symbionts links carbon and nitrogen cycling in the symbiosis. (B) aposymbiotic Aiptasia were used to quantify (C) the effect of 10 mM pyruvate addition on light $^{15}NH_4^+$ assimilation in host tissue layers using (D,E) NanoSIMS imaging. Likewise, (F) symbiotic Aiptasia were used to quantify (G) the effect of 10 mM pyruvate addition on light $^{15}NH_4^+$ assimilation in the host tissue layers as well as algal symbiont cells using (H,I) NanoSIMS imaging. Epi - epithelium, Gas - gastrodermis, Sym - algal symbionts. Asterisks indicate significant effects of pyruvate addition on ammonium assimilation in the specific tissue or cell (*** $p < 0.001$).

Algal photosynthesis alters symbiotic nitrogen availability

To test this hypothesis, we performed a long-term experiment on the effects of light availability on photosymbiotic Aiptasia. Over the course of six months, Aiptasia were gradually acclimated to seven different light levels spanning an exponential gradient from near dark (photosynthetically active radiation (PAR) < 6.25 µE s^{-1} m^{-2}) to high light intensity (PAR = 400 µE s^{-1} m^{-2}), and animals were left at their final treatment levels for one month without supplemental feeding. The lowest and highest light treatment levels exceeded the tolerance limits of a stable symbiosis. At near-dark conditions, Aiptasia exhibited a near-complete loss of algal symbionts (bleaching) while the host remained viable. At the highest light intensity, Aiptasia still hosted algal symbionts but suffered from severe host mortality (63%; Fig. S1). These symbiotic tolerance limits, i.e., PAR from 12.5 to 200.0 µE s^{-1} m^{-2}, likely reflect the tradeoffs between increasing light limitation towards the lower end of the light gradient and increasing photooxidative stress towards the higher end of the light gradient, respectively. Indeed, the role of photodamage was reflected in the maximum photosynthetic efficiency of algal symbionts declining by more than 20 % at the upper tolerance limit (PAR 200.0 µE s^{-1} m^{-2}) compared to the lower tolerance limit of the symbiosis (PAR 12.5 µE s^{-1} m^{-2}; LM, F = 62.8, $p < 0.001$; Fig. 2A**)**. In line with this, the gross photosynthetic activity of individual algal cells showed an optimum response with the highest activities at intermediate light levels, i.e., PAR 50 – 100 µE s^{-1} m^{-2} (LM, F = 3.5, $p = 0.048$; Fig. 2B**)**, and atomic carbon to nitrogen ratios (C:N ratio) of Aiptasia holobionts followed a similar pattern along the light gradient (LM, F = 5.1, $p = 0.0155$; Fig. 2C). Given that environmental nitrogen availability, i.e., dissolved seawater nutrients and heterotrophic feeding, was identical for all light treatments, these changes in the C:N ratio likely reflect the direct changes in carbon availability in the holobiont as a function of gross photosynthetic activity. Consequently, our results suggest that labile carbon availability in the symbiosis is highest under intermediate light levels and decreases towards the tolerance limits of the symbiosis at lower and higher light intensities.

The link between carbon availability and symbiotic nitrogen cycling identified above implies that algal photosynthesis should alter nitrogen assimilation in the symbiosis. Indeed, the optimum in gross photosynthesis activity and C:N ratios were consistent with a similar (albeit not significant) pattern of

daily bulk ammonium assimilation at the holobiont level based on 24 h incubations with 10 µM ^{15}N-ammonium (LM, F = 1.5, p = 0.250; Fig. 2D). To further disentangle the respective contribution of symbiotic partners to holobiont ammonium assimilation, we used NanoSIMS stable isotope imaging. This revealed that the optimum in holobiont ammonium assimilation was the composite result of the asymmetric responses of the host and algal symbiont, respectively. On average, algal symbionts showed an approximately ten-fold higher ^{15}N enrichment than the surrounding host tissue (Fig. 2E, Fig. S2A). However, algal ammonium assimilation peaked at low light availability, i.e., PAR 25 - 50 µE s^{-1} m^{-2}, while host ammonium assimilation in the gastrodermis and epidermis peaked at intermediate light levels, 50 - 100 µE s^{-1} m^{-2} (Fig. 2E, Fig. S3; algal symbionts: LM, F = 25.7, p < 0.001; host gastrodermis: LM, F = 7.8, p < 0.001; host epidermis: LM, F = 2.8, p = 0.057). While ^{15}N enrichments only reflect the uptake of environmental nitrogen in the symbiosis, the recycling of ammonium from the host catabolism is likely regulated by the same processes and follows the same patterns. High ^{15}N enrichments thus indicate a reduced production of catabolic ammonium by the host. In this light, the combined patterns of C:N ratios and ^{15}N enrichment patterns (Fig. 2C-E) imply that symbiotic competition for nitrogen is highest under intermediate light levels and decreases towards the tolerance limits of the symbiosis. Hence, our data suggest that increases in photosynthesis and associated labile carbon availability effectively enhance nitrogen limitation for algal symbionts.

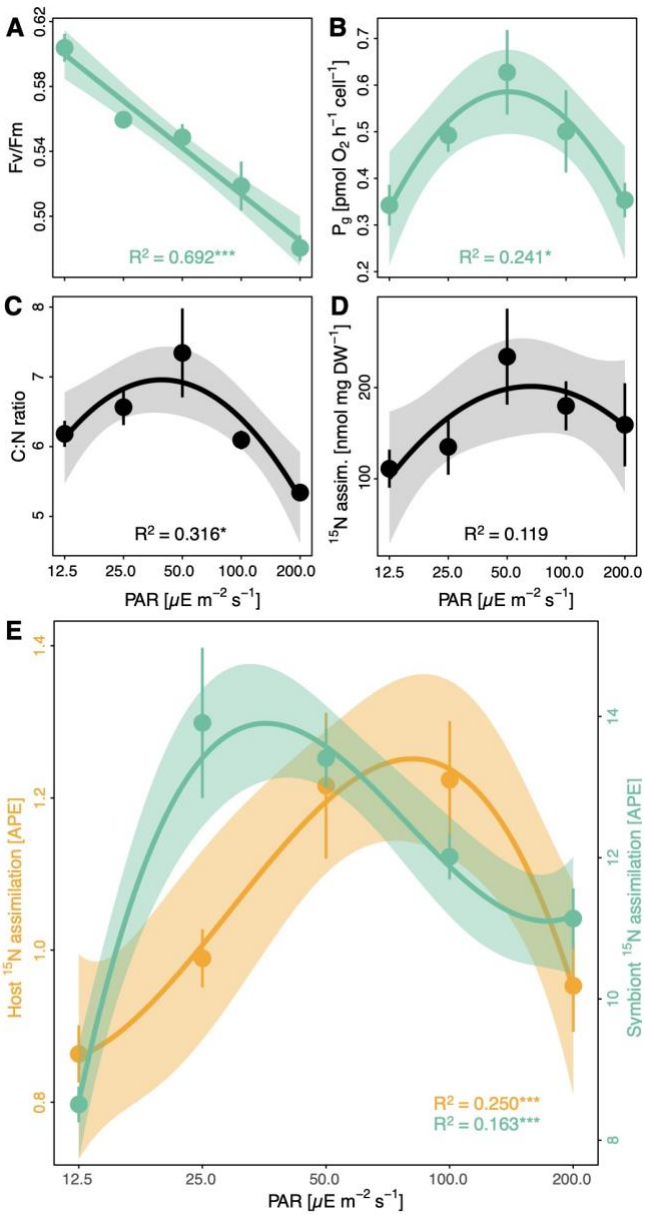

Fig. 2 | Effects of light availability on symbiotic carbon and nitrogen cycling in Aiptasia. (A) Gross photosynthesis (P_g) and **(B)** maximum quantum yield of algal symbionts. **(C)** C:N ratios, and **(D)** bulk daily $^{15}NH_4^+$ assimilation of Aiptasia holobionts (i.e., host + algae). **(E)** NanoSIMS imaging was used to disentangle $^{15}NH_4^+$ assimilation in the host gastrodermis and algal symbionts within the tolerance range of the stable symbiosis. Points and error bars indicate mean ± SE; lines represent best-fitting models with corresponding confidence intervals. R^2 values show the proportion of variance explained by the model, and asterisks indicate a significant effect of light availability on the response parameter (* p < 0.050; ** p < 0.010; *** p < 0.001).

Nitrogen availability shapes the symbiotic phenotype in Aiptasia

Given that nitrogen limitation controls algal growth in the cnidarian-algal symbiosis (15, 16, 20, 21), light-mediated changes in symbiotic nitrogen availability can directly affect the regulation of symbiosis. Indeed, light availability had a pronounced effect on the phenotype of photosymbiotic Aiptasia. Pigmentation and chlorophyll autofluorescence were at their highest levels in Aiptasia at the low and high end of the light tolerance range of the symbiosis (Fig. 3, Fig. S3B). Algal symbiont densities were lowest at 50 µE s^{-1} m^{-2} and increased by more than three-fold towards the upper and lower light tolerance limit of the symbiosis (LM, F = 8.9, p = 0.002). Likewise, chlorophyll *a* content increased by more than two-fold towards the symbiosis tolerance limits compared to intermediate light levels (LM, F = 7.9, p = 0.003). Consequently, symbiont density was lowest when their gross photosynthetic performance was highest. Indeed, algal symbiont densities showed a pronounced negative correlation with gross photosynthetic activity along the experimental light gradient (Pearson's r = -0.578, p = 0.002) and holobiont C:N ratios (Pearson's r = -0.489, p = 0.001) suggesting that the algal symbiont population is regulated by nitrogen availability (and the resulting resource competition). Under optimal environmental conditions, high photosynthetic carbon availability ensures efficient recycling of catabolic nitrogen in the host metabolism and limits nitrogen availability for algal symbionts. Under suboptimal environmental conditions, reduced carbon availability increases the relative availability of nitrogen in the holobiont thereby supporting higher symbiont densities, consistent with the feedback loop described above.

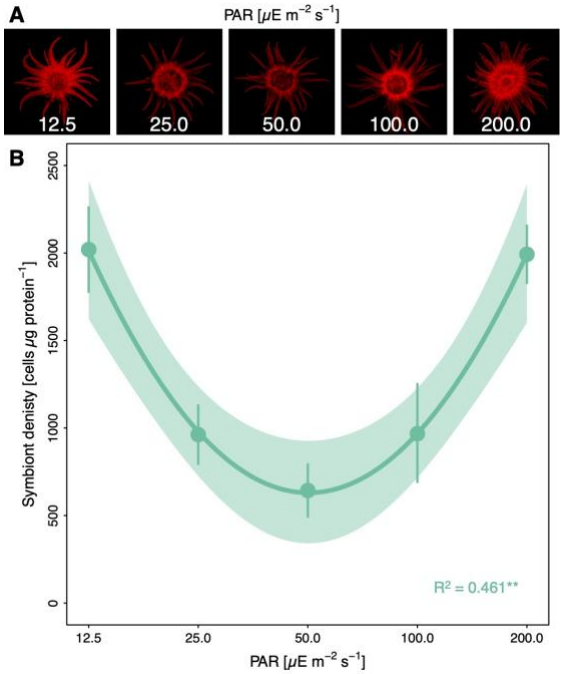

Fig. 3 | Effects of light availability on the symbiotic phenotype of Aiptasia. (A) Representative photographs of chlorophyll fluorescence of Aiptasia algal symbionts depending on light availability. **(B)** Symbiont density (green) along an exponential gradient of photosynthetic active radiation (PAR) within the tolerance range of the stable symbiosis. Points and error bars indicate mean ± SE; the line represents the best-fitting model with corresponding confidence intervals. The R^2 value shows the proportion of variance explained by the model and asterisks indicate a significant effect of light availability on the response parameter (** p < 0.010).

Nutrient cycling controls the eco-evolutionary dynamics of the cnidarian-algal symbiosis

Our results provide direct experimental support for the role of metabolic interactions in the passive regulation of the cnidarian-algal symbiosis. These findings extend previous reports and hypotheses

about the role of nutrient cycling in the eco-evolutionary dynamics of photosymbiotic cnidarians (13, 15, 19, 22, 23, 30, 35). We found that nitrogen competition between the host and its algal symbionts effectively limits nitrogen availability for algal symbionts under optimal environmental conditions. Towards the environmental tolerance limits of the symbiosis, however, this competition is gradually replaced by nitrogen competition between algal symbionts as population density increases (22). This dynamic interplay between inter- and intraspecific nitrogen competition thereby extends the tolerance range of the symbiosis by maintaining nitrogen-limited conditions across a wide range of environmental conditions. The ecological success and stability of the cnidarian-algal symbiosis may, in part, be rooted in this passive metabolic regulation of symbiotic interactions.

The regulation through resource competition implies that the relative benefits for the symbiotic partners are in an inverse relationship. Based on the data acquired here, algal symbiont densities are lowest under environmental conditions where algal symbionts provide most labile carbon to the holobiont. However, because reduced carbon translocation by algal symbionts would enhance their access to nutrients produced in the host catabolism, the observed resource competition in the symbiosis may also promote parasitic behavior by algal symbionts. While the evolution of such interactions may in part be limited by selection at the holobiont level, it is likely that, in addition to the passive metabolic regulation, an active regulation of the symbiosis is also required. To this end, so-called host-release factors that actively promote carbon release by algal symbionts could be a key component in maintaining mutualistic interactions in the cnidarian-algal symbiosis (36–38), although further data is warranted to unequivocally confirm this.

Finally, the processes described here improve our understanding of the maintenance of the symbiosis and its widespread breakdown in the Anthropocene (39). During mass bleaching events, severe and prolonged heat stress causes a dramatic loss of algal symbionts in photosymbiotic Cnidaria thereby promoting host starvation and reef degradation (40, 41). Yet, algal symbiont densities have been shown to increase prior to bleaching during early and moderate warming and corals with higher symbiont densities show increased susceptibility to bleaching (42–44). Here, we show that algal symbiont densities may increase towards the tolerance limits of the symbiosis as a consequence of reduced carbon availability for the host. Hence, an initial proliferation of algal symbionts during early heat stress is unlikely to be a beneficial response. Rather, increasing symbiont density in the early phases of environmental stress should be considered a sign of destabilization of symbiotic nutrient cycling, which might ultimately contribute to the breakdown of the symbiosis during heat stress (19, 24, 45).

Taken together, we conclude that the cnidarian-algal symbiosis is passively controlled through the coupling of carbon and nitrogen cycling in the symbiosis. Resource competition stabilizes the symbiosis under a wide range of environmental conditions. At the same time, the resulting negative relationship between the host and symbiont performance may promote the evolution of parasitic behavior and destabilize the symbiosis in times of rapid environmental change.

Material & Methods

Animal culture maintenance

All experiments were performed with "Aiptasia" clonal lineage CC7 (*sensu Exaiptasia diaphana*) (46). Prior to the experiments, the animals were reared in illuminated growth chambers (Algaetron 230, Photo System Instruments, Czech Republic) at a constant temperature of 20 °C in 2 L clear food containers (Rotho, Switzerland) filled with artificial seawater (35 PSU, Pro-Reef, Tropic Marin, Switzerland). Each week, Aiptasia anemones were fed with freshly hatched *Artemia* nauplii (Sanders GSLA, USA), thoroughly cleaned, and the seawater was exchanged. Photosymbiotic animals harboring their native algal symbiont community dominated by *Symbiodinium linuchae* strain SSA01 (Clade A4) were reared in a 12h:12h light-dark cycle with photosynthetic active radiation (PAR) of 50 µE m^{-2} s^{-1}.

Further, aposymbiotic animal cultures deprived of algal symbionts were generated following established cold shock bleaching protocols (47). Briefly, photosymbiotic animals were cold-shocked at 4 °C for 4 h followed by 8 weeks of culturing in artificial seawater containing 50 µM DCMU at constant irradiance of 50 µE m^{-2} s^{-1}. The absence of algal symbionts was confirmed using fluorescence microscopy; aposymbiotic cultures were maintained at constant darkness thereafter.

Experiment 1: effect of pyruvate on nitrogen cycling

To study the effect of labile carbon availability on symbiotic nitrogen cycling, we assessed the effect of pyruvate addition on ammonium (NH_4^+) assimilation in aposymbiotic and symbiotic Aiptasia. Following 1 week of starvation, six aposymbiotic and six photosymbiotic animals were transferred into individual 50 mL glass vials for isotope labeling. For the incubations, a minimal artificial seawater medium (35 PSU, pH 8.1, 355.6 mM NaCl, 46.2 mM $MgCl_2$, 10.8 mM Na_2SO_4, 9.0 mM $CaCl_2$, 7.9 mM, KCl, 2.5 mM $NaHCO_3$) containing 10 µM $^{15}NH_4Cl$ was used following Harrison et al. (48). While half of the animals (three aposymbiotic and three photosymbiotic) were incubated in minimal artificial seawater medium, the other half was incubated in minimal artificial seawater medium spiked with 10 mM pyruvate. Incubations were performed using the culturing conditions outlined above with aposymbiotic animals being kept in the dark and photosymbiotic animals being kept in constant light. After 6 h of incubation, all animals were immediately fixed for NanoSIMS analysis (see below).

Experiment 2: effect of light on nitrogen cycling

To study the effect of light on symbiotic nitrogen cycling, photosymbiotic animals were kept in an exponential series of irradiance levels in a long-term experiment. All seven irradiance treatments followed a 12h:12h light-dark cycle and used the same culturing conditions outlined above. Over the course of six months 30 animals per treatment were gradually acclimated in monthly steps to the following irradiance level: <6.25, 12.50, 25.00, 50.00, 100.00, 200.00, 400.00 µE m^{-2} s^{-1}. Following acclimation, animals were starved for one month to minimize confounding feeding responses on symbiotic nitrogen cycling. After this, the rate of survival of animals was recorded (any asexual offspring were removed during the weekly cleaning routines throughout the experiment). Due to severe bleaching at low and host mortality at high irradiance treatments, respectively, only mortality and symbiont densities were recorded for all irradiance treatments. All other parameters were only recorded within the tolerance range of the stable symbiosis, i.e., PAR 12.5 – 200 µE m^{-2} s^{-1}. To quantify NH_4^+ assimilation in the symbiosis, five animals per treatment were incubated in 50 mL minimal artificial seawater medium containing 10 µM $^{15}NH_4Cl$ for 24 h at their respective treatment conditions. Following the incubation, tentacles from two animals were dissected and fixed for NanoSIMS analysis, and all animals were immediately collected for bulk elemental and isotope analysis (see below). Further, the dark-adapted photosynthetic efficiency and oxygen fluxes were recorded for six and five animals per treatment, respectively (see below).

Fixation, embedding, and NanoSIMS imaging

Collected animals (experiment 1) and individual tentacles (experiment 2) were immediately transferred into a fixative solution (2.5 % glutaraldehyde and 1 % paraformaldehyde in 0.1 M Sorensen's phosphate buffer) and incubated for 1 h at room temperature followed by 24 h at 4 °C. Samples were transferred into a storage solution (1 % paraformaldehyde in 0.1 M Sorensen's phosphate buffer) and processed for dehydration and resin infiltration within four days of collection. Samples were dehydrated in a series of increasing ethanol concentrations (30 % for 10 min, 50 % for 10 min, 2 x 70 % for 10 min, 3x 90 % for 10 min, and 3 x 100 % for 10 min). For resin infiltration, samples were transferred to 100 % acetone and gradually infiltrates with Spurr resin (Electron Microscopy Sciences, USA) at increasing concentrations (25 % for 30 min, 50 % for 30 min, 75 % for 1 h, and 100% overnight), and resins were cured for 48 h at 65 °C. Embedded samples were cut into 200 nm thin sections with an Ultracut E ultra-microtome (Leica, Germany), transferred onto glow-discharged

silicon wafers, and coated with a 12 nm gold layer.

The surface isotopic composition of sample sections on silicon wafers was analyzed using a NanoSIMS 50L (Cameca, France). Following pre-sputtering for 5 minutes with a primary beam of ca. 6 pA to remove the metal coating, samples were bombarded with a 16 keV primary ion beam of ca. 2 pA Cs^+ focused to a spot size of about 150 nm on the sample surface. Secondary molecular cyanide ions $^{12}C^{14}N^-$ and $^{12}C^{15}N^-$ were simultaneously collected in electron multipliers at a mass resolution of about 9000 (Cameca definition), sufficient to resolve the $^{12}C^{15}N^-$ ions from potentially problematic interferences. Eight to nine sample areas were analyzed for each of the samples by rastering the primary beam across a 40 × 40 µm sample surface with a 256 × 256 pixels resolution and a pixel dwell time of 5 ms for five consecutive image layers. The resulting isotope maps were processed using the ImageJ plug-in OpenMIMS (https://github.com/BWHCNI/OpenMIMS/wiki). Mass images were drift and dead-time corrected, the individual planes were summed, and the $^{15}N/^{14}N$ maps were expressed as a hue-saturation-intensity image, where the color scale represents the isotope ratio. ^{15}N assimilation was recorded as atom % excess (APE, compared to unlabeled controls) by drawing regions of interest (ROIs) based on $^{12}C^{14}N^-$ maps around individual symbiont cells as well as gastrodermal (excluding symbiont cells) and epidermal tissue in each of the images (see data file (49)). In light of the clonal nature of Aiptasia and the identical environmental conditions of animals within the same treatment, individual ROIs were considered as independent measurements at the microscale level regardless of the animal replicate for the purpose of the analysis.

Bulk elemental and isotope analysis

Following collection, anemones were immediately homogenized in 1 mL MilliQ water using a Polytron PT1200E immersion dispenser (Kinematica, Switzerland), snap-frozen in liquid nitrogen, and stored at -80 °C until further analysis. Samples were freeze-dried and the dry mass was recorded for all samples. The carbon (C) to nitrogen (N) atomic ratios were quantified using a Carlo Erba 1108 elemental analyzer (Fisons Instruments, Italy). This was coupled via a Conflo III interface to a Delta V Plus isotope ratio mass spectrometer (Thermo Fisher Scientific, Germany) to determine the nitrogen isotope composition. The calibration and normalization of the measured $^{15}N/^{14}N$ ratios to the international Air-N_2 scale were performed with a dedicated set of six in-house urea standards with defined $^{15}N/^{14}N$ ratios as described in Spangenberg & Zufferey (50). To assess the ^{15}N enrichment of samples, the $^{15}N/^{14}N$ ratio was converted to atom % and converted to APE by subtracting isotopic values measured in unlabeled control animals. To quantify $^{15}NH_4^+$ assimilations by the anemones the APE was multiplied with the total nitrogen content obtained by elemental analysis and normalized to the dry weight of the sample.

Photosynthetic efficiency and gross photosynthesis

To assess the effect of light availability on the photosynthetic efficiency of algal symbionts, pulse amplitude modulated (PAM) fluorometry was used. Anemones were dark-acclimated for 1 h before the maximum quantum yield (Fv/Fm) was recorded using the blue light version of the Mini-PAM-II (Walz, Germany). For each specimen, the initial fluorescence (Fo) was recorded followed by a saturating pulse and maximum fluorescence (Fm) was measured directly afterward. The maximum quantum yield was calculated as the ratio between the variable fluorescence (Fv = Fm - Fo) and the maximum fluorescence.

To quantify gross photosynthetic rates of the anemones, respiration and net photosynthesis were measured in separate consecutive incubations. For this, anemones were transferred into 12.3 mL borosilicate vials filled with artificial seawater and equipped with an OXSP5 oxygen sensor spot (Pyroscience, Germany). Following the attachment of the animals at the vial bottom, a 6 mm magnetic stirrer was added, and each vial was sealed bubble-free, inverted, and transferred to a water bath. Vials were continuously stirred at 240 rpm using a magnetic stirring plate and oxygen concentrations

were continuously recorded with an FSO2-4 oxygen meter (PyroScience) connected via a SPFIB-BARE optical fiber (PyroScience). All incubations were performed at 20 °C for approximately 2 h each. Respiratory oxygen consumption was quantified during dark incubations. Subsequently, net photosynthetic activity was recorded during light incubations with irradiance levels according to the respective treatment conditions of the animals. Oxygen fluxes were corrected for artificial seawater control incubations and normalized to the duration of the incubation and algal symbiont consent of the animals (see below). Lastly, gross photosynthesis was calculated as the sum of the net photosynthesis rate and the absolute value of the respiration rate of each animal.

Algal symbiont densities, chlorophyll a *content, and protein content*

Following oxygen flux incubations, anemones were immediately homogenized in 0.5 mL 2x PBS using a Polytron PT1200E immersion dispenser (Kinematica), and host and symbiont fractions were separated by centrifugation (1000 g for 5 min). The host supernatant was stored at -20 °C until further analysis. The algal symbiont pellet was resuspended in 1 mL 2x PBS and divided into two equal aliquots. The first aliquot was used to quantify the concentration of algal symbiont cells in six replicate measurements using a Countess cell counter Countess II FL Automated Cell Counter (Thermo Fisher Scientific, USA) with a Cy5 light cube. Algal symbiont cells could be clearly identified by the cell counter based on their size, roundness, and chlorophyll fluorescence. The second aliquot was used for chlorophyll *a* content quantification. For this, cells were pelleted (5000 x g for 5 min), resuspended in 90 % ethanol, and incubated at 4 °C for 24 h in the dark under constant agitation. After this, cell debris was pelleted (5000 x g for 5 min) and two 200 µL supernatant per sample were transferred into a clear flat-bottom 96-well plate. Sample absorbances were immediately recorded at 630, 664, and 750 nm using a CLARIOstar Plus microplate reader (BMG Labtech, Germany), and chlorophyll content was calculated according to Jeffrey & Humphrey (51):

$$\text{Chlorophyll } a\ [\mu g\ mL^{-1}] = 11.43 \times (OD_{664} - OD_{750}) - 0.644 \times OD_{630}\ (-OD_{750}).$$

Symbiont densities and chlorophyll *a* content were normalized against host tissue protein content as a proxy of host biomass. Protein content in the defrosted host supernatant was quantified according to Bradford (52). Three technical 5 µL replicates were analyzed for each sample using the Pierce Coomassie (Bradford) Protein Assay Kit (Thermo Scientific, US) according to the manufacturer's instruction, and the absorbance of samples, as well as BSA calibration standards, was recorded at 595 nm using a CLARIOstar Plus microplate reader (BMG Labtech).

Statistical analysis

For the first experiment, data from the host and symbiont compartments were analyzed separately. NanoSIMS data were square root transformed to meet model assumptions, and the effects of symbiotic state (aposymbiotic vs. photosymbiotic) and treatment (control vs. pyruvate addition) were tested in a two-way analysis of variance (ANOVA) followed by Tukey's honest significance test.

For the second experiment, only measurements within the defined tolerance range of the stable symbiosis, i.e., PAR 12.5 – 200 µE m^{-2} s^{-1}, were used for the statistical analysis. All data were analyzed using linear regression models (LM) using irradiance treatment levels as an explanatory variable. Where necessary, a second-degree (symbiont density, gross photosynthesis, C:N ratio, bulk ^{15}N assimilation) or third-degree (NanoSIMS measurements for host tissues and symbiont cells) polynomial transformation was applied to the data to meet model assumptions. Further, Pearson correlations were used to test the linear relationship between gross photosynthesis rates and symbiont densities.

Acknowledgments

We are grateful to Kristin Bär-Hage, Myriam Schmid, and Petra Merkel for their help with culture

maintenance at the University of Konstanz. Dr. Michael Laumann and Dr. Paavo Bergmann from the Electron Microscopy Centre at the University of Konstanz are thanked for their assistance with sample preparation. N.R. and A.M. were supported by the Swiss National Science Foundation, grants 200021_179092 and 205321_212614.

References

1. F. Not, *et al.*, "Photosymbiosis in marine pelagic environments" in *The Marine Microbiome: An Untapped Source of Biodiversity and Biotechnological Potential*, L. J. Stal, M. S. Cretoiu, Eds. (Springer International Publishing, 2016), pp. 305–332.

2. M. D. Brasier, J. F. Lindsay, A billion years of environmental stability and the emergence of eukaryotes: new data from northern Australia. *Geology* **26**, 555–558 (1998).

3. J. Decelle, S. Colin, R. A. Foster, "Photosymbiosis in marine planktonic protists" in *Marine Protists: Diversity and Dynamics*, S. Ohtsuka, T. Suzaki, T. Horiguchi, N. Suzuki, F. Not, Eds. (Springer Japan, 2015), pp. 465–500.

4. G. D. Stanley Jr, Photosymbiosis and the evolution of modern coral reefs. *Science* **312**, 857–858 (2006).

5. K. Frankowiak, *et al.*, Photosymbiosis and the expansion of shallow-water corals. *Sci Adv* **2**, e1601122 (2016).

6. T. P. Hughes, *et al.*, Global warming and recurrent mass bleaching of corals. *Nature* **543**, 373–377 (2017).

7. L. Muscatine, J. W. Porter, Reef corals: mutualistic symbioses adapted to nutrient-poor environments. *Bioscience* **27**, 454–460 (1977).

8. P. G. Falkowski, Z. Dubinsky, L. Muscatine, J. W. Porter, Light and the bioenergetics of a symbiotic coral. *Bioscience* **34**, 705–709 (1984).

9. N. Rädecker, C. Pogoreutz, C. Wild, C. R. Voolstra, Stimulated respiration and net photosynthesis in *Cassiopeia* sp. during glucose enrichment suggests *in hospite* CO_2 limitation of algal endosymbionts. *Front. Mar. Sci.* **4**, 16 (2017).

10. Z. Dubinsky, P. L. Jokiel, Ratio of energy and nutrient fluxes regulates symbiosis between zooxanthellae and corals. *Pacific Science* **48**, 313–324 (1994).

11. R. Cunning, E. B. Muller, R. D. Gates, R. M. Nisbet, A dynamic bioenergetic model for coral-*Symbiodinium* symbioses and coral bleaching as an alternate stable state. *J. Theor. Biol.* **431**, 49–62 (2017).

12. L. P. Suescún-Bolívar, G. M. I. Traverse, P. E. Thomé, Glycerol outflow in *Symbiodinium* under osmotic and nitrogen stress. *Mar. Biol.* **163**, 128 (2016).

13. P. G. Falkowski, Z. Dubinsky, L. Muscatine, L. McCloskey, Population control in symbiotic corals. *Bioscience* **43**, 606–611 (1993).

14. D. Yellowlees, T. A. V. Rees, W. Leggat, Metabolic interactions between algal symbionts and invertebrate hosts. *Plant Cell Environ.* **31**, 679–694 (2008).

15. T. Xiang, *et al.*, Symbiont population control by host-symbiont metabolic interaction in Symbiodiniaceae-cnidarian associations. *Nat. Commun.* **11**, 108 (2020).

16. G. Cui, *et al.*, Nutritional control regulates symbiont proliferation and life history in coral-dinoflagellate symbiosis. *BMC Biol.* **20**, 103 (2022).

17. M. Mies, P. Y. G. Sumida, N. Rädecker, C. R. Voolstra, Marine invertebrate larvae sssociated with *Symbiodinium*: a mutualism from the start? *Frontiers in Ecology and Evolution* **5** (2017).

18. C. Pogoreutz, *et al.*, Sugar enrichment provides evidence for a role of nitrogen fixation in coral bleaching. *Glob. Chang. Biol.* **23**, 3838–3848 (2017).

19. N. Rädecker, *et al.*, Heat stress destabilizes symbiotic nutrient cycling in corals. *Proceedings of the National Academy of Sciences* **118**, e2022653118 (2021).

20. N. Rädecker, C. Pogoreutz, C. R. Voolstra, J. Wiedenmann, C. Wild, Nitrogen cycling in corals: the key to understanding holobiont functioning? *Trends Microbiol.* **23**, 490–497 (2015).

21. L. A. Morris, C. R. Voolstra, K. M. Quigley, D. G. Bourne, L. K. Bay, Nutrient Availability and Metabolism Affect the Stability of Coral–Symbiodiniaceae Symbioses. *Trends Microbiol.* **27**, 678–689 (2019).

22. T. Krueger, *et al.*, Intracellular competition for nitrogen controls dinoflagellate population density in corals. *Proc. Biol. Sci.* **287**, 20200049 (2020).

23. G. Cui, *et al.*, Host-dependent nitrogen recycling as a mechanism of symbiont control in Aiptasia. *PLoS Genet.* **15**, e1008189 (2019).

24. D. M. Baker, J. P. Andras, A. G. Jordán-Garza, M. L. Fogel, Nitrate competition in a coral symbiosis varies with temperature among *Symbiodinium* clades. *ISME J.* **7**, 1248–1251 (2013).

25. S. E. McIlroy, C. P. terHorst, M. Teece, M. A. Coffroth, Nutrient dynamics in coral symbiosis depend on both the relative and absolute abundance of Symbiodiniaceae species. *Microbiome* **10**, 192 (2022).

26. G. Puntin, *et al.*, Harnessing the power of model organisms to unravel microbial functions in the coral holobiont. *Microbiol. Mol. Biol. Rev.*, e0005322 (2022).

27. S. Baumgarten, *et al.*, The genome of Aiptasia, a sea anemone model for coral symbiosis. *Proc. Natl. Acad. Sci. U. S. A.* **112**, 11893–11898 (2015).

28. O. Rahav, Z. Dubinsky, Y. Achituv, P. G. Falkowski, D. C. Smith, Ammonium metabolism in the zooxanthellate coral, *Stylophora pistillata*. *Proceedings of the Royal Society of London. B. Biological Sciences* **236**, 325–337 (1989).

29. M. Pernice, *et al.*, A single-cell view of ammonium assimilation in coral–dinoflagellate symbiosis. *ISME J.* **6**, 1314–1324 (2012).

30. G. Cui, *et al.*, Molecular insights into the Darwin paradox of coral reefs from the sea anemone Aiptasia. *bioRxiv* (2022).

31. G. Cui, *et al.*, Nitrogen competition is the general mechanism underlying cnidarian-Symbiodiniaceae symbioses. *bioRxiv*, 2022.06.30.498212 (2022).

32. E. Gibbin, G. Banc-Prandi, M. Fine, A. Comment, A. Meibom, A method to disentangle and quantify host anabolic turnover in photosymbiotic holobionts with subcellular resolution. *Commun Biol* **3**, 14 (2020).

33. J. C. Danne, S. G. Gornik, J. I. Macrae, M. J. McConville, R. F. Waller, Alveolate mitochondrial metabolic evolution: dinoflagellates force reassessment of the role of parasitism as a driver of change in apicomplexans. *Mol. Biol. Evol.* **30**, 123–139 (2013).

34. N. Rädecker, *et al.*, Using Aiptasia as a model to study metabolic interactions in cnidarian-*Symbiodinium* symbioses. *Front. Physiol.* **9**, 214 (2018).

35. N. F. Strumpen, N. Rädecker, C. Pogoreutz, A. Meibom, C. R. Voolstra, High light quantity suppresses locomotion in symbiotic Aiptasia. *Symbiosis* **86**, 293–304 (2022).

36. K. J. T. Withers, A. J. Grant, R. Hinde, Effects of free amino acids on the isolated symbiotic algae of the coral *Plesiastrea versipora* (Lamarck): absence of a host release factor response. *Comp. Biochem. Physiol. A Mol. Integr. Physiol.* **120**, 599–607 (1998).

37. A. Grant, J. People, M. Rémond, S. Frankland, R. Hinde, How a host cell signalling molecule modifies carbon metabolism in symbionts of the coral *Plesiastrea versipora*. *FEBS J.* **280**, 2085–2096 (2013).

38. R. D. Gates, O. Hoegh-Guldberg, M. J. McFall-Ngai, K. Y. Bil, L. Muscatine, Free amino acids exhibit anthozoan "host factor" activity: they induce the release of photosynthate from symbiotic dinoflagellates in vitro. *Proc. Natl. Acad. Sci. U. S. A.* **92**, 7430–7434 (1995).

39. T. P. Hughes, *et al.*, Spatial and temporal patterns of mass bleaching of corals in the Anthropocene. *Science* **359**, 80–83 (2018).

40. C. A. Oakley, S. K. Davy, Cell biology of coral bleaching. *Ecological Studies*, 189–211 (2018).

41. O. Hoegh-Guldberg, Climate change, coral bleaching and the future of the world's coral reefs. *Mar. Freshwater Res.* **50**, 839–866 (1999).

42. R. Cunning, A. C. Baker, Excess algal symbionts increase the susceptibility of reef corals to bleaching. *Nat. Clim. Chang.* **3**, 259–262 (2012).

43. K. B. Strychar, M. Coates, P. W. Sammarco, Loss of *Symbiodinium* from bleached Australian scleractinian corals (*Acropora hyacinthus*, *Favites complanata* and *Porites solida*). *Marine and Freshwater Research* **55**, 135 (2004).

44. G. Grimsditch, J. Mwaura, J. Kilonzo, N. Amiyo, D. Obura, High zooxanthellae densities and turnover correlate with low bleaching tolerance in Kenyan corals (2008) (November 12, 2022).

45. K. Petrou, B. L. Nunn, M. P. Padula, D. J. Miller, D. A. Nielsen, Broad scale proteomic analysis of heat-destabilised symbiosis in the hard coral *Acropora millepora*. *Sci. Rep.* **11**, 19061 (2021).

46. S. Sunagawa, *et al.*, Generation and analysis of transcriptomic resources for a model system on the rise: the sea anemone *Aiptasia pallida* and its dinoflagellate endosymbiont. *BMC Genomics* **10**, 258 (2009).

47. P. Lab, "Cold-shock protocol to bleach Aiptasia" (Protocols.io, 2018) https:/doi.org/10.17504/protocols.io.qx8dxrw (October 20, 2022).

48. P. J. Harrison, R. E. Waters, F. J. R. Taylor, A broad spectrum artificial sea water medium for coastal and open ocean phytoplankton. *J. Phycol.* **16**, 28–35 (1980).

49. N. Rädecker, S. Escrig, J. E. Spangenberg, C. R. Voolstra, A. Meibom, Data for "Coupled carbon and nitrogen cycling regulates the cnidarian-algal symbiosis" (2022) https:/doi.org/10.5281/ZENODO.7404865.

50. J. E. Spangenberg, V. Zufferey, Carbon isotope compositions of whole wine, wine solid residue, and wine ethanol, determined by EA/IRMS and GC/C/IRMS, can record the vine water status-a comparative reappraisal. *Anal. Bioanal. Chem.* **411**, 2031–2043 (2019).

51. S. W. Jeffrey, G. F. Humphrey, New spectrophotometric equations for determining chlorophylls a, b, c1 and c2 in higher plants, algae and natural phytoplankton. *Biochemie und Physiologie der Pflanzen* **167**, 191–194 (1975).

52. M. M. Bradford, A rapid and sensitive method for the quantitation of microgram quantities of protein utilizing the principle of protein-dye binding. *Anal. Biochem.* **72**, 248–254 (1976).

Supplementary Figures

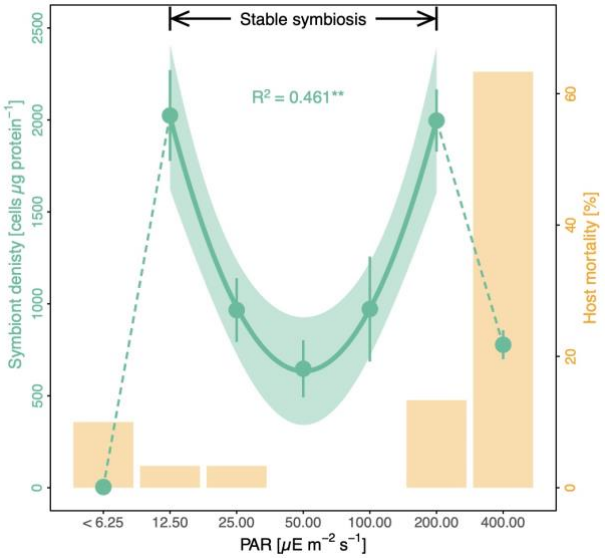

Fig. S1 | Effects of light availability on symbiont density (green) and host mortality (yellow) in Aiptasia. Points and error bars indicate mean ± SE; the line represents the best-fitting model with corresponding confidence intervals. R^2 values show the proportion of variance explained by the model, and asterisks indicate a significant effect of light availability on the response parameter (** $p < 0.010$).

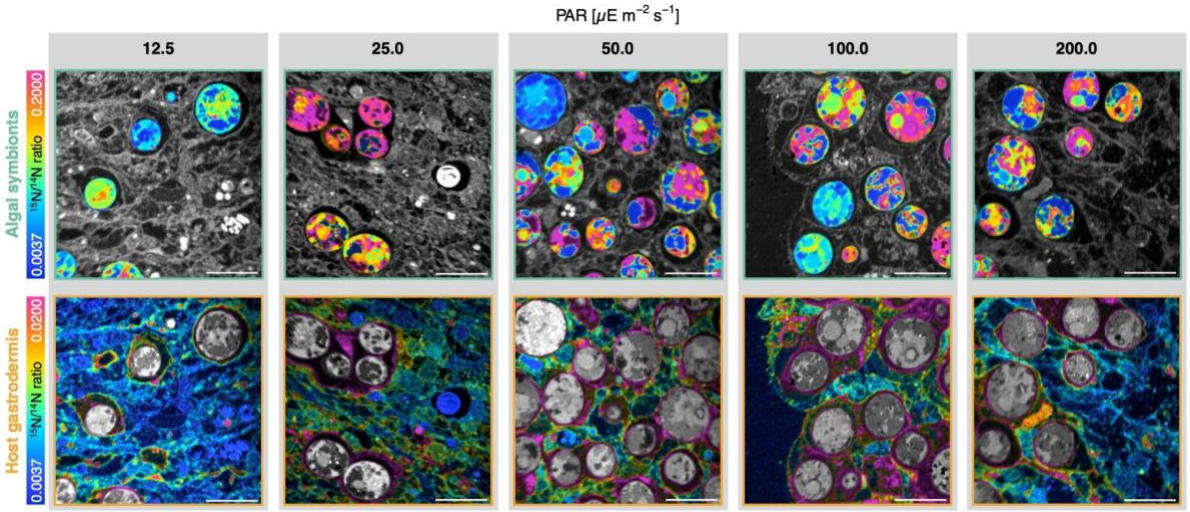

Fig. S2 | Exemplary NanoSIMS images illustrating the effect of light availability on $^{15}NH_4^+$ assimilation in Aiptasia. The top row shows hue saturation images of $^{15}N/^{14}N$ ratios for algal symbionts with surrounding host tissue shaded in gray. The bottom row shows hue saturation images of $^{15}N/^{14}N$ ratios for host gastrodermis with algal symbionts shaded in gray. Note the different scales for the top and bottom rows. Scale bars are 10 µm.

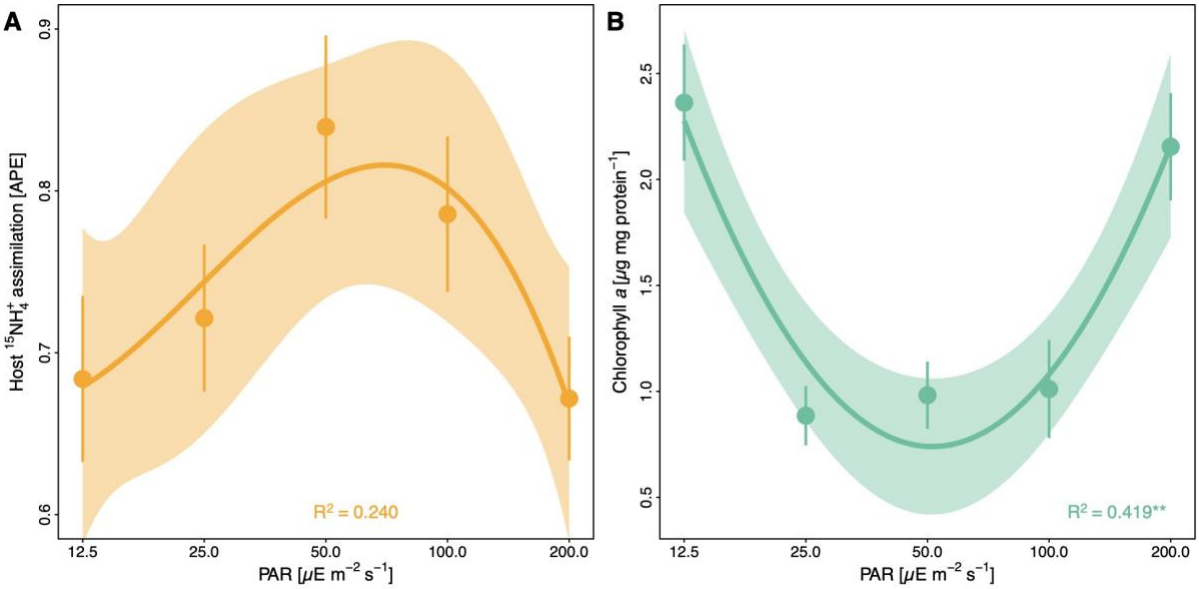

Fig. S3 | Effects of light availability on (A) epidermal $^{15}NH_4^+$ assimilation and (B) chlorophyll *a* content in Aiptasia. Points and error bars indicate mean ± SE; lines represent the best-fitting models with corresponding confidence intervals. R^2 values show the proportion of variance explained by the respective model, and asterisks indicate a significant effect of light availability on the response parameter (** $p < 0.010$).